

## COMPUTER SIMULATION OF HIGH FREQUENCY MODULATION OF LASER DIODE RADIATION

E. Šermukšnis, J. Vyšniauskas, T. Vasiliauskas, and V. Palenskis

*Department of Radiophysics, Vilnius University, Saulėtekio 9, LT-10220 Vilnius, Lithuania*

E-mail: juozas.vysniauskas@ff.vu.lt, vilius.palenskis@ff.vu.lt

Received 7 July 2004

Dynamic characteristics in the case of a large signal of partly gain-coupled multiple-quantum-well InGaAsP–InP distributed feedback (GC DFB) laser diodes have been investigated. Simple rate equations for carrier and photon densities were taken. A possibility to simulate the modulation characteristics of GC DFB lasers using these equations has been shown. Chirp and optical power pulses obtained by time-resolved frequency chirp measurements were compared with modelled ones.

**Keywords:** computer simulation, laser diodes, time-resolved frequency chirp, relative intensity noise (RIN)

**PACS:** 42.55.Px

### 1. Introduction

Optical devices emitting at 1.5  $\mu\text{m}$  wavelength are suitable for long haul and high bit rate optical data transmission systems. Laser diode (LD) acts as a key element in such systems. Narrow linewidth, high direct modulation speed, and low cost are preferable. Partly gain-coupled (GC) distributed feedback (DFB) laser diodes show better performance as compared to index-coupled ones [1]: they have high single-mode yield, high side-mode suppression ratio, reduced spatial hole burning, and reduced sensitivity to the external optical feedback, low frequency chirp, large intrinsic modulation bandwidth, good long-term reliability. The permanent increase of data transmission rate requires the development of new LD structures. A simulation of laser physical processes is very relevant today because it can help to better understand the operation of such devices.

### 2. Investigated devices

The object of computer simulation was a partly gain-coupled distributed feedback InGaAsP–InP multiple-quantum-well semiconductor laser where the gain coupling is achieved by periodic cutting of several quantum wells along the active region [2]. A first-degree grating cuts two or three quantum wells. The active region of measured semiconductor lasers consists of six undoped InGaAsP compressively strained (1.3%) layer quantum wells and five lattice-matched  $p$ -doped

InGaAsP barriers. Below and above the active region there are separate confinement layers.

### 3. Experimental results

Time-resolved frequency chirp and relative intensity noise (RIN) measurements were done in order to estimate LD's dynamic characteristics. The bias current was modulated at a 2.5 Gbit/s rate by a rectangular pulse generator, and pulse characteristics were measured. DC and current pulse amplitude values were chosen such that the mean optical power and the extinction rate were 5 mW and 8.5 dB, respectively. The electrical signal was passed through a microwave cable and applied directly to the laser microwave input strip line using a microwave RF probe. A biased T-coupler was connected to the RF line and direct current was applied using the same microwave probe. The investigated samples were fed from low noise current sources. For light beam coupling a tapered fibre was precisely positioned near the laser output facet so that reflections from the fibre input lens were minimal with respect to coupled power. The Advantest Q7606B Optical Chirpform Test Set with the built-in Mach–Zehnder interferometer and the Tektronix TDS800 digital sampling oscilloscope with an optical input block were used for further modulated optical beam chirp measurements. By arranging the interferometer, two different interferometer frequency transfer function areas can be chosen and two different waveforms AM + FM and

AM – FM can be loaded to the digital scope. Here AM and FM mean the optical beam power modulation and the optical beam frequency modulation terms. The frequency transfer function has a sinusoidal shape, therefore, frequency deviation  $\Delta f$  can be calculated in such a way:

$$\Delta f = \frac{\text{FSR} \sin^{-1}(V_{\text{FM}}/V_{\text{AM}})}{2\pi}, \quad (1)$$

where FSR is the free spectral range of the interferometer,  $V_{\text{AM}}$  is the amplitude modulation term,  $V_{\text{FM}}$  is the frequency modulation term [3].

Laser's main mode frequency deviations during direct current modulation are referred to as a frequency chirp [3, 4]. Chirp dependence on time is usually referred to as a time-resolved chirp. Optical beam power waveforms can be found from time-resolved chirp measurements as well.

Data acquired with the scope is averaged over 1024 samples and the software digital frequency filter is applied to reduce signal transmission and digital scope noise. Relative intensity noise (RIN) was measured using HP electrical spectrum analyser in the frequency range from 0.5 to 22 GHz. Since laser RIN is very sensitive to reflections, an optical isolator was applied. Thermal and shot noises were measured using an HP supplied routine (for the HP-70004A controller).

Room-temperature measurements were made at a different bias up to 80 mA, while coupled power was not exceeding 0 dBm.

Relaxation–oscillation frequency  $f_r$  and damping  $\Gamma$  were evaluated by fitting the RIN dependence on the frequency curve:

$$\text{RIN}(f) = \frac{A + Bf^2}{(f_r^2 - f^2) + [\Gamma/(2\pi)]f^2}, \quad (2)$$

where  $A$  and  $B$  are the fitting constants, and  $f$  is the frequency [5]. Linear fitting of oscillation–relaxation and damping frequencies versus the bias current was done in the low bias current region (lower than 40 mA) in order to achieve better accuracy.

#### 4. Computer simulation results

The emitted optical power is proportional to the photon density in the active region and the chirp is proportional to the carrier density [4]. Typical optical power and time-resolved chirp pulses are shown in Fig. 1.

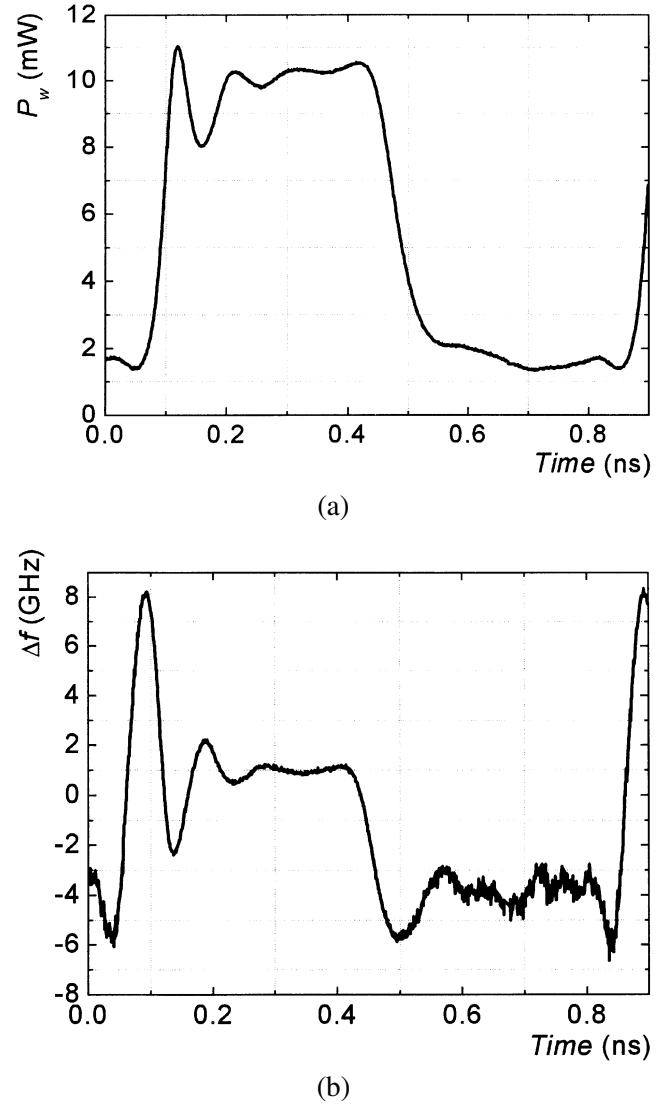


Fig. 1. (a) Optical power and (b) chirp pulses obtained from the time-resolved frequency chirp measurements.

Ordinary rate equations for the carrier and photon density were used to describe the LD dynamic behaviour [5]. For carrier density the equation is

$$\frac{dn}{dt} = \frac{J}{ed} - \frac{n}{\tau_s} - \alpha(n - n_{\text{ot}})p, \quad (3)$$

where  $n$  is the carrier density in the active region,  $p$  is the photon density. Here we use the bias current density  $J$ ,  $d$  is the active region width,  $\tau_s$  represents the carrier lifetime, and  $\alpha$  is the differential optical gain,  $n_{\text{ot}}$  is the carrier density at transparency. The rate equation for the photon density is

$$\frac{dp}{dt} = \alpha(n - n_{\text{ot}})p - \frac{p}{\tau_p} + \beta \frac{n}{\tau_s}, \quad (4)$$

where  $\tau_p$  is the photon lifetime and  $\beta$  is the spontaneous emission factor. The first term on the right-hand

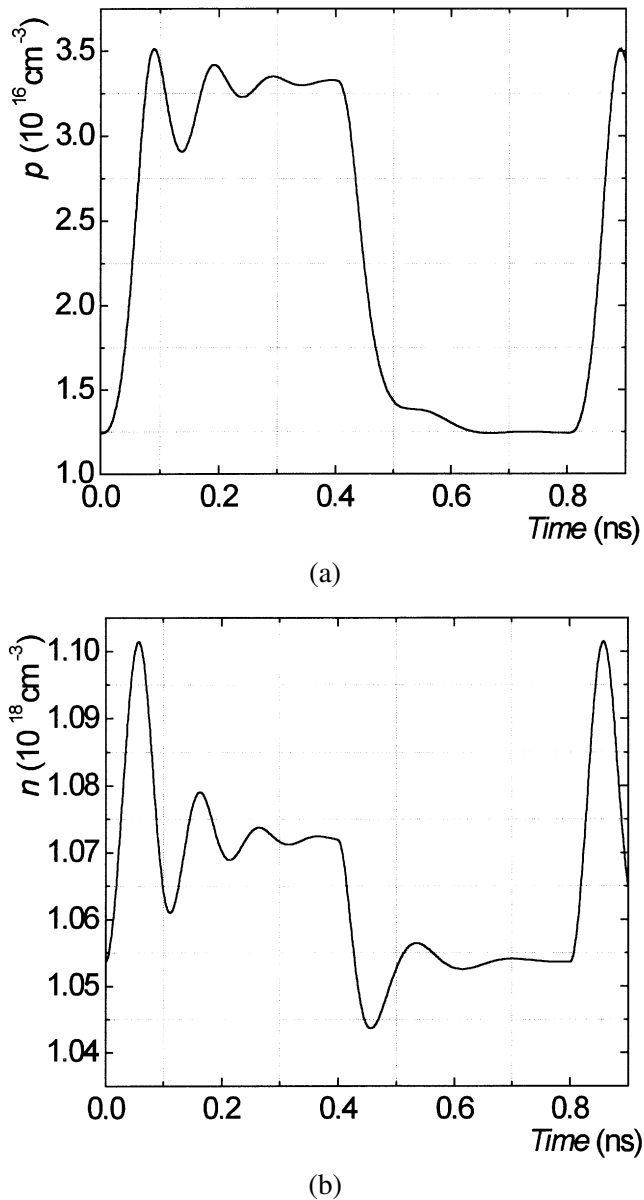


Fig. 2. Modelled (a) photon and (b) carrier density pulses.

side of Eq. (3) accounts for injected carriers, the second for losses of carriers due to spontaneous recombination. There  $\alpha(n - n_{ot})$  describes optical gain. The term  $p/\tau_p$  describes both the photon loss through facets and the absorption in the active region. Part of photons are emitted spontaneously, that is why the last term is present in Eq. (4).

For simplicity, the optical gain is supposed to be linear and dependent only on carrier density. Carrier lifetime is supposed to be constant, i. e. independent of carrier density.

Various differential equation solving methods, such as Euler's method or the fourth-order Runge–Kutta method, can be used to simulate numerically the

dynamic characteristics of LDs. Different methods can have various modelling accuracy and computation time. These two methods were compared and it was found that the Runge–Kutta method is preferable. If the time step  $\Delta t$ , which was used for modelling, is about  $10^{-14}$  s, both methods give the same accuracy. But in the case when  $\Delta t = 4 \cdot 10^{-12}$  s, the accuracy of Euler's method became obviously worse while the accuracy of the Runge–Kutta method did not change. If these equations describe the actual device operation quite well, then, by selecting the proper simulation parameters, one should obtain that the simulated photon and carrier pulses match the experimental pulses. These fittings were varied until the best match between the simulated and experimental data was reached (compare Figs. 1 and 2).

Variation of the parameter  $\alpha$  obviously changes the carrier and photon density oscillation amplitude, large signal oscillation frequency, and damping. Carrier densities at '0' and '1' levels (see Fig. 3) depend on parameter  $\alpha$  while photon densities at these levels are almost constant. The oscillation amplitude for both carrier and photon densities has a maximum, as can be seen in Fig. 3. The oscillation frequency shows nearly  $f_r^2 \sim \alpha$  dependence for both the carrier and photon densities. Damping shows similar behaviour to that as well. The main purpose of the coefficient  $\alpha$  variation was an accurate oscillation frequency matching. This model fits experiment best when  $\alpha = 6 \cdot 10^{-7}$  cm<sup>3</sup>/s for laser pulses in Fig. 1. In this case the differences between modelled and measured photon and carrier oscillation frequencies were 0.5% and 4.2%, respectively.

The product of carrier and photon lifetime was taken such that these two parameters would correspond to the actually possible LD values. It was noticed that by changing  $\tau_p$  and  $\tau_s$  values the '0' and '1' levels for both  $p$  and  $n$  varied. The dependence of the carrier as well as photon density oscillation amplitude on the photon lifetime has a maximum. In the case of the carrier density oscillation amplitude maximum the photon lifetime is equal to 5 ps, while the photon density oscillation amplitude reaches its maximum when the photon lifetime is equal to 10 ps. The large signal oscillation frequency of carrier and photon densities depends on the photon lifetime as well. The main criterion for choosing both lifetimes was the best match between the simulated and measured carrier and photon densities at levels '0' and '1'. For the measured LD (Fig. 1) these parameters were taken as  $\tau_s = 3.82 \cdot 10^{-9}$  s and  $\tau_p = 5 \cdot 10^{-12}$  s, respectively.

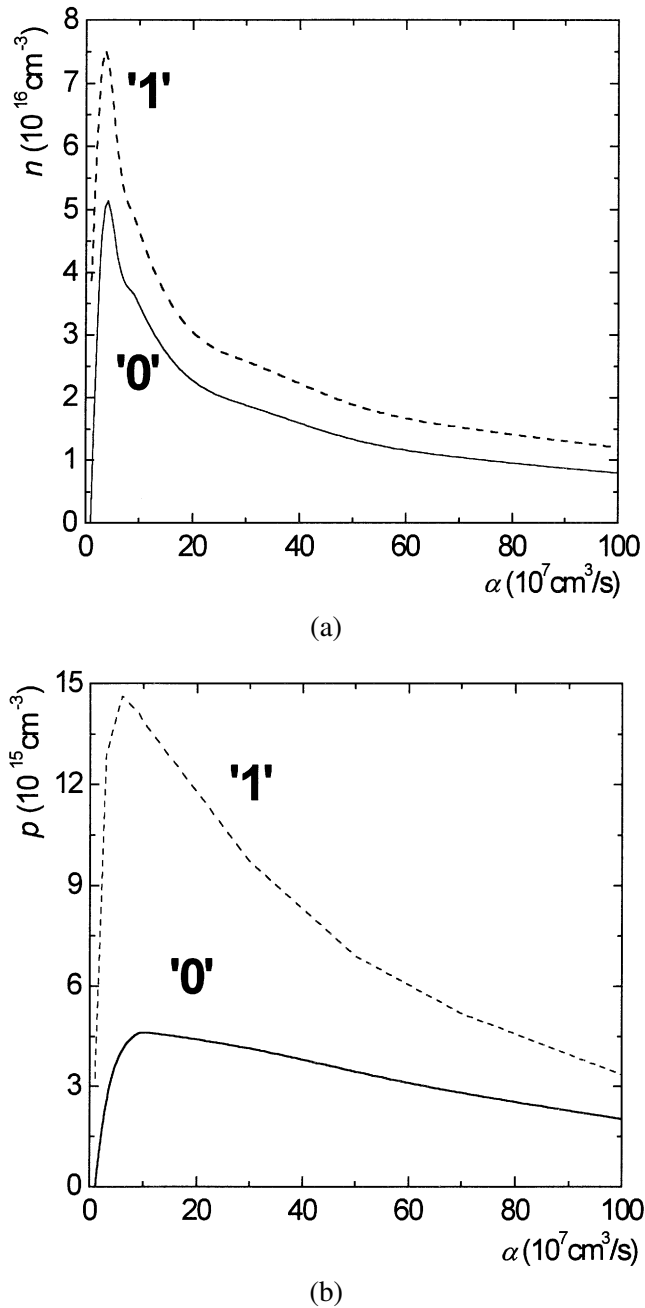


Fig. 3. The dependence of (a) carrier and (b) photon density oscillation amplitude on parameter  $\alpha$  for both '0' and '1' levels in the case of a large signal.

The spontaneous emission factor  $\beta$  was also varied in a wide range. The main effects of  $\beta$  variation were the changes in the oscillation amplitude and damping frequency. It also has a weak effect on the variation of the carrier density at '0' and '1' levels. Spontaneous emission factor variation helps to finally match the oscillation amplitude and damping, while the oscillation frequency stays almost constant.

In the model it was supposed that bias current pulses are strictly of a rectangular shape. In the experiment

it was very problematic to measure the laser's real bias current pulse. On the one hand, this is related to the small laser input dimensions and partly to the nonideal laser interface and RF probe impedance matching. On the other hand, simulated pulses showed that the introduction of a semirectangular pulse could substantially improve simulated and experimental data matching. Two kinds of pulses were tested, a bell-shaped pulse and pulse with exponential trailing edges. The latter pulse showed obviously better matching.

Several LDs were simulated and dynamic parameters were extracted. For some samples, the simulated and measured pulses matched quite well. Computer simulation difficulties appeared mostly for samples with the higher damping frequency and the smaller oscillation amplitude. It is consistent with the small-signal theory, where relaxation–oscillation and damping frequencies are described in terms of such laser dynamic parameters as the carrier and photon lifetime, differential gain, and nonlinear gain. Large damping in the LD can be achieved by introducing nonlinear gain.

Relative intensity noise measurements of the LD optical beam were carried out and some dynamic parameters were extracted. Some of them were compared to those obtained by modelling. Oscillation–relaxation frequency square  $f_r^2$  versus bias  $I$  dependence was obtained from RIN dependences on the bias current [5]. Small-signal analysis predicts that at least in the small current region, where nonlinear or thermal effects do not appear,  $f_r^2$  should be proportional to the bias current [5]:

$$f_r^2 = D(I - I_{th}) = D(\Delta I), \quad (5)$$

where the parameter  $D$  is the square frequency gradient versus bias current, and  $I_{th}$  is the threshold current. The parameter  $D$  can be rewritten in another form:

$$D = \frac{G_N}{q} = \frac{\Gamma v_g g_n}{Vq}, \quad (6)$$

where  $G_N$  is the differential gain per second,  $q$  is the electron charge,  $\Gamma$  represents the fact that the optical mode spatial dimension is larger than the active region volume  $V$  and is referred to as the mode confinement factor. Further,  $v_g$  is the group velocity, and  $g_n$  is the differential gain per centimetre.

By small-signal harmonic current source simulation, the LD transfer function can be calculated and the oscillation–relaxation frequency dependence on the constant bias current can be found. Figure 4 shows that the transfer function has resonant behaviour, and the

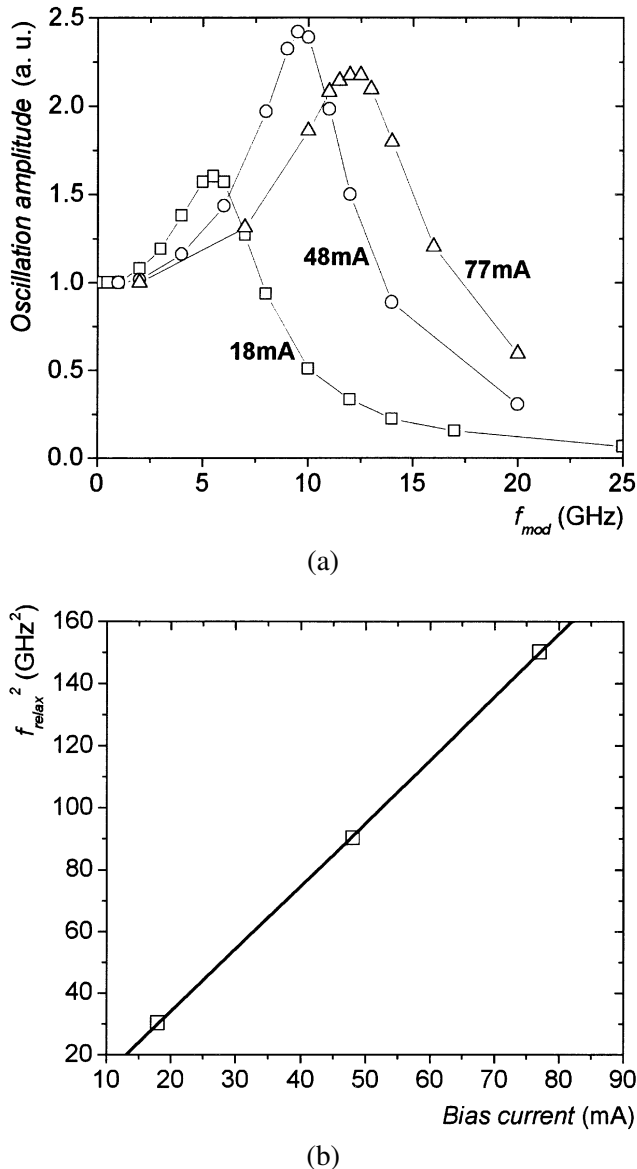


Fig. 4. (a) The simulated LD transfer function corresponding to different bias current, and (b) the transfer function resonant square frequency dependence on the bias current.

peak frequency increases together with DC bias. Peak frequency square versus bias current shows linear dependence. It is the same behaviour as that of the real LD. The peak frequency in Fig. 4 corresponding to the current pulse '1' level is nearly the same as the large signal photon density oscillation in Figs. 1 and 2, and in both cases the frequency is approximately equal to 10 GHz. From the peak square frequency versus bias current slope the parameter  $D$  can be found. In this case  $D$  is equal to  $2 \text{ GHz}^2/\text{mA}$ . Model parameter  $\alpha$ , which also appears in Eqs. (3) and (4), is proportional to the parameter  $D$  in Eq. (5). The parameter  $D$  ex-

tracted by the RIN measurement was proportional to the parameter  $\alpha$ .

## 5. Conclusions

Simulation of bias current modulation of InGaAsP laser diodes in the case of a large signal was carried out. Time-resolved frequency chirp and relative intensity noise measurements were done. The frequency chirp pulse, which in form is proportional to the carrier density time pulse, and the optical power pulse, which is proportional to the photon density time pulse, were obtained. Carrier and photon density pulses were simulated using the same boundary conditions for rate equations as the measured pulses had. It was shown that transient processes in the distributed feedback semiconductor lasers could be described and simulated by simple rate equations within about 5% tolerance even if some important processes had not been accounted for. By varying such model parameters as the carrier and photon lifetime, differential optical gain, and spontaneous emission factor, the simulated pulses matched the measured ones. The best results were obtained for samples where the carrier and photon oscillation amplitude was larger and the damping was lower, i. e. in the samples with negligible nonlinear gain effect on the pulse form. Frequency transfer function simulation shows that the simulated oscillation frequency coincides well with that obtained from relative intensity noise measurements.

## References

- [1] H. Lu, T. Makino, and G.P. Li, Dynamic properties of partly gain-coupled  $1.55\text{-}\mu\text{m}$  DFB lasers, *IEEE J. Quantum Electron.* **31**, 1443–1450 (1995).
- [2] H. Lu, G.P. Li, and T. Makino, High-speed performance of partly gain-coupled  $1.55\text{-}\mu\text{m}$  strained layer multiple-quantum-well DFB lasers, *IEEE Photon. Technol. Lett.* **5**, 861–863 (1993).
- [3] R.A. Saunders, J.P. King, and I. Hardcastle, Wideband chirp measurement technique for high bit rate sources, *Electron. Lett.* **30**, 1336–1338 (1994).
- [4] C.H. Henry, Theory of the linewidth of semiconductor lasers, *IEEE J. Quantum Electron.* **QE-18**, 259–264 (1982).
- [5] M.C. Tatham, I.F. Lealman, C.P. Seltzel, L.D. Westbrook, and D.M. Cooper, Resonance frequency, damping and differential gain in  $1.5 \mu\text{m}$  multiple quantum-well lasers, *IEEE J. Quantum Electron.* **28**, 408–414 (1992).

## KOMPIUTERINIS LAZERINIŲ DIODŲ SPINDULIUOTĖS AUKŠTADAŽNĖS MODULIACIJOS MODELIAVIMAS

E. Šermukšnis, J. Vyšniauskas, T. Vasiliauskas, V. Palenskis

*Vilniaus universitetas, Vilnius, Lietuva*

### Santrauka

Ištirtos InGaAsP lazerinių diodų (LD) su daugeliu kvantinių duobių bei paskirstytu grįžtamoju ryšiu dinaminės charakteristikos, esant stipriam signalui. Išmatuoti LD spinduliuotės galios fliktuacijų normuotas spektrinis tankis (NST) bei pašalinė dažninė moduliacija (PDM). NST išmatuotas dažnių srityje nuo 0,5 iki 22 GHz, esant skirtingam LD srovės stipriui. Aproximuojant eksperimentinį NST žinoma teorine priklausomybe, surasti diferencialinis optinis stiprinimas, relaksacinių virpesių dažnis, slenksinės srovės stipris bei kai kurie kiti lazerių veikos parametrai. PDM išmatuota interferometrinio būdu, esant 2,5 Gbit/s LD srovės moduliacijos spartai. Parodyta puslaidininkinių lazerių su paskirstytu grįžtamoju ryšiu dinaminės charakteristikų modeliavimo galimybė. Žinant LD PDM bei spinduliuotės galios impulsų vertes, kompiuteriu buvo sumodeliuota aukštadažnė spinduliuotės moduliacija. Modeliavimui panaudotos supaprastintos elektronų ir fotonų tankio kitimo lygtys, kuriose nebuvo atsižvelgta į

netiesinį optinį stiprinimą. Taip pat, sprendžiant elektronų tankio kitimo lygtį, laikyta, kad krūvininkų gyvavimo trukmė nepriklauso nuo jų tankio. Parodyta, kad, naudojant ir supaprastintą modelį, gauti modeliniai ir eksperimentiniai optinės galios impulsai bei PDM gana gerai sutampa: skirtumai neviršija kelių procentų. Papildomai buvo sumodeliuotos LD dažninės perdavimo charakteristikos, esant skirtingai LD srovei. Iš dažnių charakteristikų rasta tiesinė relaksacinių virpesių dažnio kvadrato priklausomybė nuo srovės stiprio. Panašios tiesinės priklausomybės buvo gautos ir iš NST eksperimentinių rezultatų priklausomybės nuo LD srovės. Buvo pastebėta, kad silpno signalo relaksacinių virpesių dažnis sutampa su stipraus impulsinio signalo virpesių dažniu. Taip pat parodyta, kad kai kuriais atvejais, modeliuojant eksperimentines LD impulsines spinduliuotės charakteristikas, galima surasti dinaminis parametrus, kaip ir naudojant įprastinius NST ir panašius silpnų signalų matavimo metodus.